FastMag: A 3-D Magnetostatic Inductance Extraction Program for Structures with Permeable Materials

Yehia Massoud
Synopsys Inc.
Mountain View, CA

Jacob White
MIT
Cambridge, MA

Abstract

In this paper we present a fast and efficient program for extraction of the frequency dependent inductance of structures with permeable materials. The program, FastMag, uses a magnetic surface charge formulation, efficient techniques for evaluating the required integrals, and a preconditioned GMRES method to solve the resulting linear system. Results from examples are presented to demonstrate the accuracy and versatility of the FastMag program.

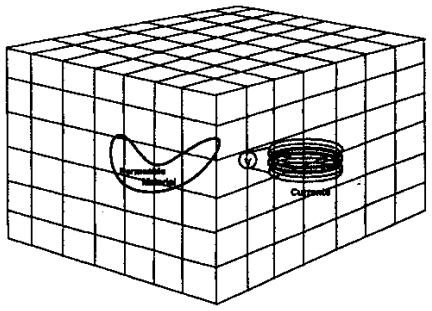

Figure 1: Finite difference discretization of all of space

1 Introduction

Permeable materials have been used in many of today's Micro-Electro-Mechanical Structures, MEMS, such as, micromotors [1], planar inductors [2, 3], and magnetic force based actuators [4, 5] to increase the device's inductance, and consequently, the force generated by the device. Permeable materials have been also used in magnetic micro power applications to miniaturize various electronic devices including inductors and transformers [6, 7].

A common approach to extract the inductance for these structures is to apply a finite difference or finite element method to the governing equations in differential form. Such an approach generates a global mesh for all parts of the analyzed structure and for the surrounding external space. This causes the number of unknowns to increase significantly, and thus, a very large linear system can be generated, as shown in Figure 1. Solving this large generated linear system requires excessive memory and CPU time, making the analysis of complex 3-D permeable structures impractical.

In this paper, we develop a fast algorithm for efficient extraction of the frequency dependent inductance of structures with magnetic materials. The approach used is based on including fictitious magnetic surface charges [8, 9, 10]. The approach also avoids computing fields inside the permeable materials, as these small fields are difficult to compute accurately due to numerical cancellation errors. This approach is more efficient than finite element methods as it only requires discretization of the current carrying conductors and the surfaces of the magnetic materials.

In Section 2, the integral formulation and integral evaluation schemes used in FastMag are reviewed. In Section 3, we described a preconditioned GMRES method which is up to an order of magnitude faster than a standard direct method. In Section 4, we present computational experiments that demonstrate the convergence characteristics and the accuracy of our approach. Finally, in Section 5, we summarize the work presented in the paper.

2 Integral Formulation Background

2.1 Equivalent Magnetic Problem

For many problems in MEMS, one can assume that regions that contain permeable materials are separated from current carrying conductors, as shown in Figure 2. For such problems, it is possible to use a fictitious magnetic charge method in which the conductors are divided into filaments over which the current is assumed constant, and the permeable material surface is divided into panels over which the magnetic charge is assumed constant [8]. Using this approach the magnetic problem becomes equivalent to the free space problem, as shown in Figure 3.

0-7803-7607-2/02/$17.00 © 2002 IEEE

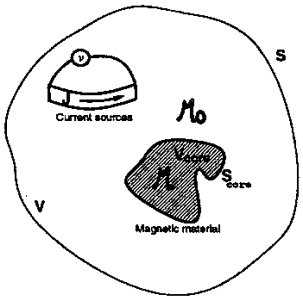

Figure 2: Current sources are outside the magnetic material

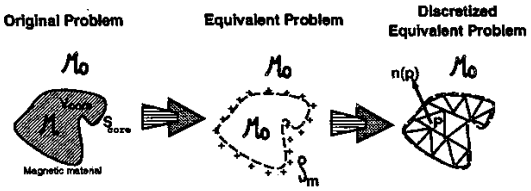

Figure 3: Linear magnetic material can be represented with an equivalent free space problem with magnetic surface charges distributed on the magnetic material interfaces. The interface is discretized into panels on which charge is assumed constant

The fictitious magnetic charge can be determined from the equation for the jump in the normal magnetic field at the permeable material interface as in,

$$\rho_m(r)\frac{2\pi(\mu_r+1)}{(\mu_r-1)} = \nabla \times \int_v \frac{J(r')dv' \cdot n(r)}{\mid r-r' \mid} - \int_s \rho_m(r')n(r) \cdot \nabla \frac{1}{\mid r-r' \mid} dS'_{core} \quad (1)$$

where ρ_m is the fictitious surface charge density, S_{core} is the surface of the magnetic material, μ_r is the magnetic material's relative permeability, J is the current density, and n(r) is the unit vector normal to the magnetic material surface calculated at point r. Note that the second term of (1) represents the normal magnetic field due to currents, and the third term represents the normal magnetic field due to fictitious magnetic charges.

The conductor current satisfies an integral equation derived using a modified vector potential which includes the effect of the magnetic material on the current distribution as in,

$$\frac{J(r)}{\sigma} + \frac{j\omega\mu}{4\pi}\int_V' \frac{J(r')}{\mid r-r' \mid} dv' + \frac{j\omega\mu}{4\pi}\nabla_r \int_{S'_m} \frac{-\rho_m(r')}{\mid r-r' \mid} dS'_m = -\nabla\phi(r) \quad (2)$$

where S_m is the surface of the permeable material, and ϕ is the scalar potential. Note that the second term and the third term of (2), divided by $j\omega\mu$, represent the vector potential due to the currents and the the vector potential due to fictitious magnetic charges, respectively.

In order to solve these two coupled integral equations(1) and (2), we discretized the surface of the magnetic material into panels and the current carrying conductors into filaments that are then combined into loops. By using these loop and panel basis functions to represent the currents and charges, we converted (1) and (2) to the following system that could be solved numerically [8]:

$$\begin{bmatrix} R(\omega)+j\omega L_J(\omega) & j\omega L_\rho(\omega) \\ Hn_J & (Hn_\rho - I) \end{bmatrix} \begin{bmatrix} \overline{I}_M \\ \overline{q}_m \end{bmatrix} = \begin{bmatrix} V \\ 0 \end{bmatrix} \quad (3)$$

where I_M, V, and q_m are the loop current vector, loop voltage vector, and q_m is the fictitious magnetic charge density vector, respectively.

2.2 Evaluation of R and L_J

A general element in the loop resistance sub-matrix R can be directly computed using

$$R_{ij} = \sum_{f=1}^{\#filaments\ in\ mesh\ j} \frac{1}{\sigma a_f} \int_{L_i} \mathbf{l_i} \cdot \mathbf{l_f}\, dL \quad (4)$$

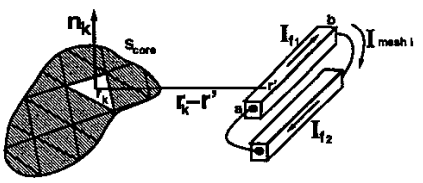

Figure 4: Evaluating $[Hn_J]_{ki}$, the magnetic field due to current mesh i, at point r_k, dotted with the unit normal to panel k, n_k.

A general element in the loop inductance sub-matrix L_J is given by

$$L_{J_{ij}} = \sum_{f=1}^{\#fil.\ in\ mesh\ j} \frac{j\omega\mu_0}{4\pi a_f} \int_{L_i} \int_{V_f'} \frac{\mathbf{l_i} \cdot \mathbf{l_f}}{|\vec{r} - \vec{r}'|} dV'\, dL \quad (5)$$

where σ is the conductivity, V_f' is the volume of filament f in mesh j, $\mathbf{l_i}$ is the unit length along the length of the i^{th} mesh, a_f is the cross sectional area of filament f, $\mathbf{l_f}$ is the unit length along the length of the filament, f, and L_i is the length of the i^{th} mesh.

The elements in (5) can be computed using analytical formulas for partial mutual inductance and partial self inductance of rectangular filaments [11].

2.3 Evaluation of Hn_ρ and Hn_J

A general element in the sub-matrix Hn_J in the linear system (3), $[Hn_J]_{ki}$, is the magnetic field due to current mesh i, at point r_k, dotted with the unit normal to panel k, n_k, as shown in Figure 4. $[Hn_J]_{ki}$ is the sum of line integrals over all the filaments that constitute mesh i, as in

$$[Hn_J]_{ki} = \sum_{f=1}^{\#fil.\ in\ mesh\ i} G_{kf} = \frac{j\omega\mu_0}{2\pi} \frac{\mu_r - 1}{\mu_r + 1} * \sum_{f=1}^{\#fil.\ in\ mesh\ i} \int_{L_{fil.\ f}} \nabla \frac{1}{|r_k - r'|} \times \mathbf{l_f} \cdot n_k dl' \quad (6)$$

where $\mathbf{l_f}$ is the unit vector along the length of filament f. Each element, G_{kf}, in the summation in (6) can be calculated analytically by transforming each filament into the panel coordinates [8].

A general element in the sub-matrix Hn_ρ in the linear system (3), $[Hn_\rho]_{pk}$, is the magnetic field due to the magnetic charge of panel k, dotted with the unit normal to panel p, $n(p)$, is given by,

$$[Hn_\rho]_{pk} = \frac{j\omega\mu_0}{2\pi a_k} \frac{\mu_r - 1}{\mu_r + 1} \int_{S_p} \int_{S_k} \nabla \frac{1}{|r - r'|} \cdot n(p) dS_k dS_p \quad (7)$$

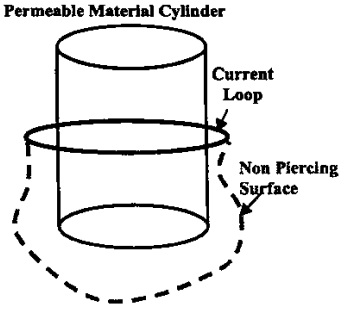

Figure 5: A non Piercing current loop surface. The surface should avoid cutting the permeable material in order to avoid numerical cancellation errors.

where S_k and S_p are the surfaces of panels k and p, respectively, and a_k is the area of panel k. The above integral is approximated using a qualocation scheme [9].

2.4 Evaluating $[L_\rho]_{ki}$

The matrix element $[L_\rho]_{ki}$ corresponds to the impact of magnetic charge on panel k on the current in loop i and is given by:

$$[L_\rho]_{ki} = -\frac{j\omega\mu_0}{4\pi} \int_{S_{loop\ i}} \nabla \frac{1}{|r - r'|} \cdot n(r) dS, \quad (8)$$

where n(r) is the normal to the surface of current loop i at point r and $S_{loop\ i}$ is the non-piercing surface bounded by the filaments in loop i. In order to avoid numerical cancellation errors, the surface should be non-piercing. That is, the surface should not penetrate the magnetic material, as shown in Figure 5. Constructing "non-piercing" surfaces for arbitrary geometries of conductors and permeable material structures can be very difficult, but the problem can be avoided by converting the surface integral into a line integral [10].

3 Preconditioned GMRES

Gaussian elimination is a standard method to solve linear systems such as the one in (3). Since (3) is dense, Gaussian elimination is computationally very expensive as it requires order n^3 operations, where n is the number of unknowns. For complicated MEMS structures, n is more than several thousands, and therefore, dense Gaussian elimination becomes too expensive. For this reason we used the krylov-subspace based iterative method GMRES [12]. The computational cost of using GMRES is order kn^2, where k is the number of iterations needed to achieve convergence. Clearly GMRES will be less expensive if few iterations are needed to achieve convergence.

As is well-known, GMRES convergence can be significantly accelerated by using a preconditioner. A good preconditioner should be an accurate approximation of the inverse of the system matrix yet be inexpensive to compute. We used a right preconditioner matrix, P, with which we were effectively using GMRES to solve

$$\left(\begin{bmatrix} R(\omega) + j\omega L_J(\omega) & j\omega L_\rho(\omega) \\ Hn_J & (Hn_\rho - I) \end{bmatrix} [P] \right) [x] = \begin{bmatrix} V \\ 0 \end{bmatrix} \quad (9)$$

for the unknown vector x. We then compute $\begin{bmatrix} \overline{I}_M \\ \overline{q}_k \end{bmatrix}$ using the matrix vector product, Px.

Since the individual elements in the sub-matrix Hn_ρ in (3) decay like $\frac{1}{r^2}$, the sub-matrix $[Hn_\rho - I]$ has its largest entries on the diagonal. Note that the diagonal elements of Hn_ρ are zeros, thus, the identity matrix produces a good approximation of the sub-matrix $[Hn_\rho - I]$. The elements of coupling sub-matrix Hn_J are the field values on the panels. These values are, at largest, of the same order as the elements of Hn_ρ which is dominated by the identity. Moreover, the elements of the sub-matrix $j\omega L_\rho$ decay like $\frac{1}{r^2}$ which is much faster than the $\frac{1}{r}$ decay of the elements of $j\omega L_J$. Thus, the sub-matrices Hn_J and $j\omega L_\rho$ are small and are ignored in the preconditioner. The above argument suggests that a good P would be:

$$P = \begin{bmatrix} lp^{-1} & 0 \\ 0 & -I \end{bmatrix} \quad (10)$$

where lp^{-1} is an approximation to the sub-matrix $[R(\omega) + j\omega L_J(\omega)]^{-1}$. The sub-matrices R and L_J are related to the partial inductance model [13, 14, 15] via the following equations

$$\begin{aligned} L &= ML_pM^t \\ R &= MR_pM^t \end{aligned} \quad (11)$$

where M is the sparse mesh matrix, L_p is the $N_f \times N_f$ partial inductance matrix, with N_f is the total number of filaments. R_p is the $N_f \times N_f$ diagonal matrix of filament DC resistances.

Note that lp^{-1} should be a good approximation to $[MR_p(\omega)M^t + j\omega ML_pM^t(\omega)]^{-1}$. If we get a sparsified approximation of L_p, we can then get a sparse matrix lp, and thus a sparse preconditioner, P, using (10) will be formed.

The simplest sparse approximation of L_p is the diagonal, but that approximation excludes the tight interaction between clusters of filaments used to model the non-uniform current distribution associated with the skin effect. To address this problem, the block diagonals of L_p associated with different conductor sections are used as a preconditioner [15].

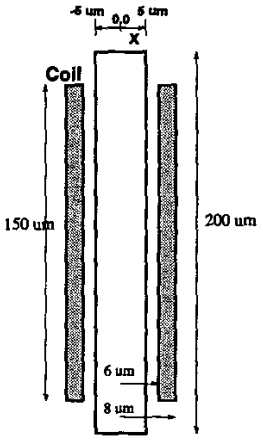

Figure 6: Coil surrounding $\mu_r = 1000$ cylinder.

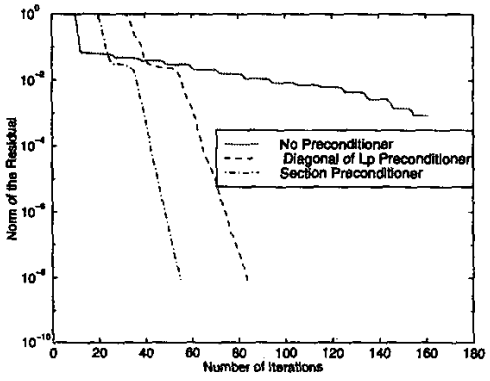

Figure 7: Convergence of GMRES using different preconditioners, for the problem of the cylindrical inductor with permeable core. The linear system size is 1765 by 1765.

4 Algorithm Results

In Figure 7, we show the convergence rate of the FastMag program when extracting the inductance of of the cylindrical coil with permeable core shown in Figure 6. We see that the section preconditioner converges faster than the diagonal of L_p method and that both of them are much faster GMRES with no preconditioner.

Figure 7 shows the number of GMRES iterations needed to extract the inductance of the cylindrical coil with permeable core shown in Figure 6. As it is illustrated Figure 8, using a preconditioner significantly reduced the number of iterations in the GMRES algorithm. A good preconditioner helps keep the number of iterations almost constant with the increase of the number of unknowns, as it is the case for the section block diagonal preconditioner.

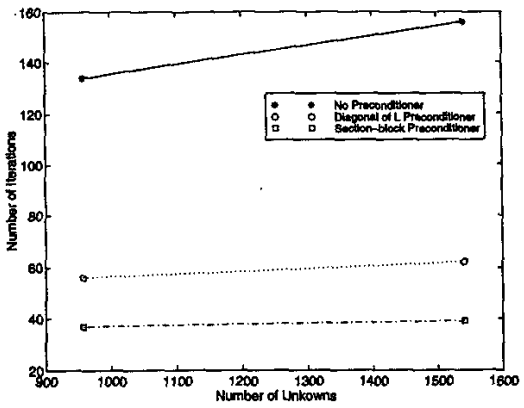

Figure 8: Effect of preconditioner on the number of iterations used in GMRES for the cylindrical inductor example.

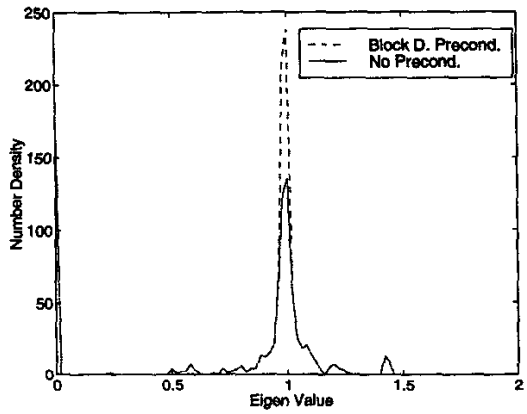

Figure 9: Eigen values for the preconditioned system and the un-preconditioned system. Note the many near-zero eigen values for the un-preconditioned system

The faster convergence of GMRES when using the section block diagonal preconditioner can be explained by examining the eigen value distributions of the preconditioned system matrix and the un-preconditioned system matrix in Figure 9. The eigen values for the preconditioned system are much more clustered than in the un-preconditioned system. Moreover, there are many more near-zero eigen values in the un-preconditioned system. These near zero eigen values imply that the matrix is ill conditioned, and therefore, GMRES converges slowly [16].

We used the industrial example of a microfabricated inductor in [17] to further test the convergence rate of our preconditioned GMRES algorithm. The microfabricated inductor is shown in Figure 10, 11. We used

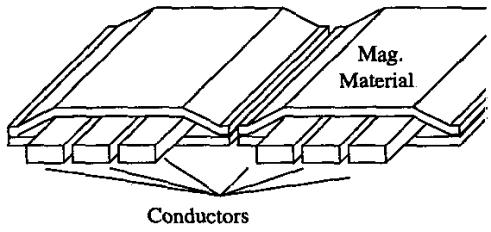

Figure 10: Side view of the microfabricated inductor

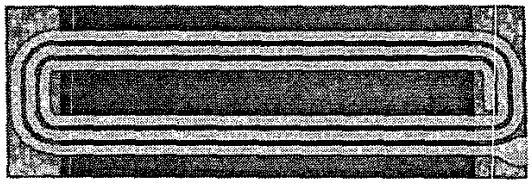

Figure 11: Top view of the multi layer core microfabricated inductor

the section block diagonal preconditioner to accelerate the convergence rate of GMRES. For a resulting linear system of 2905×2905, the section preconditioner significantly improved the convergence compared to not using a preconditioner, as shown in Figure 12.

In Figure 13, we show the CPU time consumed when solving the cylindrical inductor with the preconditioned GMRES method and with the standard direct methods such as Gaussian Elimination. Figure 13 shows that the preconditioned GMRES method using the section preconditioner is up to an order of magnitude faster than standard Gaussian Elimination method.

An example to demonstrate the accuracy of the algorithm is the standard test example of a spiral planar inductor over a permeable material substrate. The tested realistic spiral inductor in Figure 14 has a diameter of 280μ, with a 10μ by 10μ cross section. The permeable material substrate is 1500μ by 1500μ, with 200μ as its thickness. Figure 15 shows the variation of extracted inductance with the permeability of the permeable substrate. The inductance of the spiral inductor over a magnetic substrate increases as the permeability increases, until it reaches an upper limit which is almost double the value of the spiral inductance without a substrate. This matches very well the theoretical analysis in [18]. Figure 16 shows the frequency response of the inductance of the spiral inductor in Figure 14. Note the high frequency inductance is lower than the low frequency one, due to the skin effect.

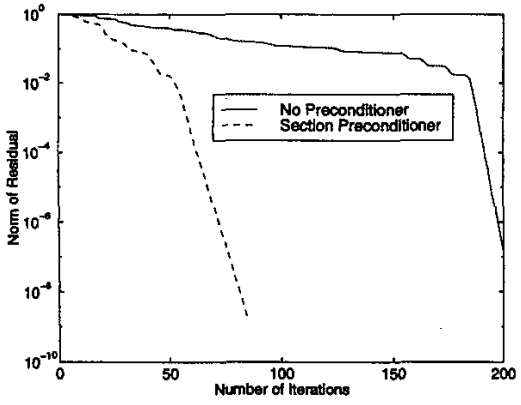

Figure 12: Much Improved GMRES convergence rate when using section preconditioner for the microfabricated inductor

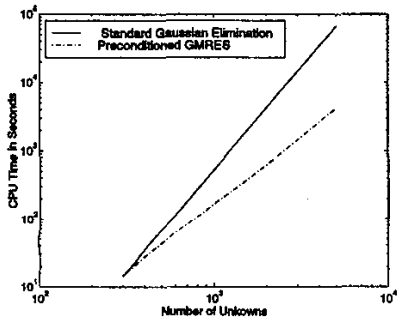

Figure 13: Comparison between the CPU times consumed in the preconditioned GMRES method and in the standard direct method.

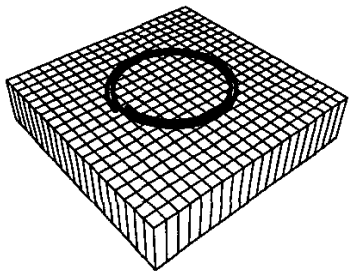

Figure 14: A spiral inductor over a magnetic substrate. The spiral inductor has a diameter of 280μ, with a 10μ by 10μ cross section. The permeable material substrate is 1500μ by 1500μ, with 200μ as its thickness.

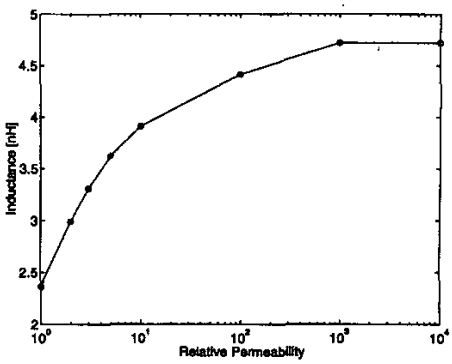

Figure 15: Variation of the inductance of spiral inductor with relative of the magnetic substrate.

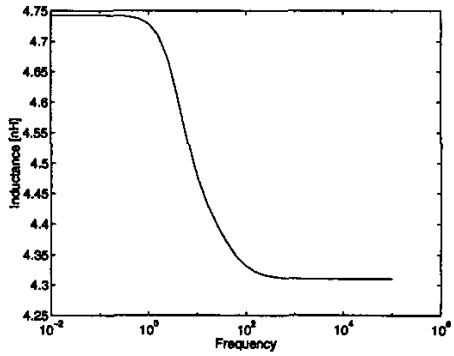

Figure 16: Inductance frequency response of the spiral inductor over a magnetic substrate example. The substrate has a relative permeability of 2000.

5 Conclusions

In this paper, we presented FastMag, a fast algorithm to efficiently extract the frequency dependent inductance for 3-D structures that contain permeable materials. The algorithm uses a magnetic surface charge formulation and efficient techniques for evaluating the required integrals. This algorithm avoids numerical cancellation errors by calculating fields outside of the permeable material. Computational results were presented to demonstrate the accuracy and the speed of our algorithm. The resulting system is solved iteratively using a preconditioned GMRES method that is up to an order of magnitude faster than the standard direct method, and therefore, facilitate the analysis of complicated structures.

This work was supported by Synopsys Inc., and by the MEMS Macromodeling Program of the Defense Advanced Research Projects Agency, the National Science Foundation.

References

[1] H. Guckel, T. Christenson, K. Skrobis, T. Jung, J. Klein, K. Hartojo, and I. Widjaja, "A first functional current excited planar rotational magnetic micromotor," *IEEE Transactions on Micro-Electromechanical Systems*, pp. 7–11, January 1993.

[2] C. Ahn and M. Allen, "Micromachined planar inductors on silicon wafers for mems applications," *IEEE Transactions on Industrial Electronics*, pp. 866–876, December 1998.

[3] C. Ahn, Y. Kim, and M. Allen, "A fully integrated planar toroidal inductor with a micromachined nickel-iron magnetic bar," *IEEE Transactions on Components Packaging and Manufacturing Technology Part A*, pp. 463–469, September 1994.

[4] W. Taylor, O. Brand, and M. Allen, "Fully integrated magnetically actuated micromachined relays," *Journal of Microelectromechanical Systems*, pp. 181–191, June 1998.

[5] C. Ahn and M. Allen, "A planar micromachined spiral inductor for integrated magnetic microactuator applications," *Journal of Micromechanics and Microengineering*, pp. 37–44, June 1993.

[6] C. Sullivan and S. Sanders, "Design of microfabricated transformers and inductors for high-frequency power conversion," *IEEE Transactions on Power Electronics*, pp. 228–238, February 1996.

[7] T. Sato, H. Tomita, A. Sawabe, T. Inoue, T. Mizoguhci, and M. Sahashi, "A magnetic thin film inductor and its application to a MHZ switching dc-dc converter," *IEEE Transactions on Micro-Electromechanical Systems*, pp. 217–223, March 1994.

[8] Y. Massoud and J. White, "Fast inductance extraction of 3-d structures with non-const permeabilities," in *Proceedings of the International Conference on Modeling and Simulation of Microsystems*, April 1998.

[9] Y. Massoud, J. Wang, and J. White, "Accurate inductance extraction with permeable materials using qualocation," in *Proceedings of the International Conference on Modeling and Simulation of Microsystems*, April 1999.

[10] Y. Massoud and J. White, "Improving the generality of the fictitious magnetic charge approach to computing inductances in the presence of permeable materials," in *Proceedings of the Design Automation Conference*, June 2002.

[11] F. W. Grover, *Inductance Calculations, Working Formulas and Tables.* New York: Dover Publications, 1962.

[12] Y. Saad and M. H. Schultz, "GMRES: A generalized minimal residual algorithm for solving nonsymmetric linear systems," *SIAM Journal on Scientific and Statistical Computing*, vol. 7, pp. 856–869, July 1986.

[13] W. T. Weeks, L. L. Wu, M. F. McAllister, and A. Singh, "Resistive and inductive skin effect in rectangular conductors," *IBM Journal of Res. and Develop.*, vol. 23, pp. 652–660, November 1979.

[14] A. E. Ruehli, "Inductance calculations in a complex integrated circuit environment," *IBM J. Res. Develop.*, vol. 16, pp. 470–481, September 1972.

[15] M. Kamon, M. Tsuk, and J. White, "Fasthenry: A mutipole-accelerated 3-d inductance extraction program," *IEEE Transactions on Microwave Theory and Techniques*, pp. 1750–1758, September 1994.

[16] G. H. Golub and C. F. V. Loan, *Matrix Computations.* Baltimore: The Johns Hopkins University Press, 1989.

[17] L. Daniel, C. Sullivan, and S. Sanders, "Design of Microfabricated Inductors," *IEEE Transactions on Power Electronics*, vol. 14, July 1999.

[18] W. Roshen and D. Turcotte, "Effect of finite thickness of magnetic substrate on planar inductors," *IEEE Transactions on Magnetics*, pp. 270–275, January 1990.